JOURNAL OF INFORMATION SECURITY AND APPLICATIONS ■■ (2016) ■■–■■

Available online at www.sciencedirect.com

ScienceDirect

journal homepage: www.elsevier.com/locate/jisa

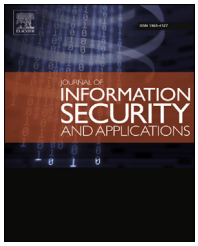

Enhancing embedding capacity and stego image quality by employing multi predictors

A.H.M. Kamal [*,1], *Mohammad M. Islam* [1]

Department of Computer Science and Engineering, Bangladesh University of Engineering and Technology, Dhaka, Bangladesh

ARTICLE INFO

Article history:
Available online

Keywords:
Multi-predictor
Prediction error
Hybrid error
Optimal error
Reversible embedding scheme
Embedding capacity and error histogram

ABSTRACT

Prediction error based reversible schemes, which are of a category of single layer data embedment process, conceal message bits mostly into two distinct embeddable errors, e.g. 0 and –1. In the single layer data embedment schemes, the embeddable errors conceive message bit of '0' and '1' through shifting their values by zero and one unit respectively, while the non-embeddable errors must change their values by one just to assist a process of performing reversibility. Hence, the resulting distortions in the stego image overwhelmingly increase along with the rises in the quantity of non-embeddable errors. Increasing the quantity of embeddable errors, thus, enhances both the embedding space and the stego image quality. The authors in this paper enhance the process of increasing the number of embeddable errors –1 and 0 through employing multi predictors, say n predictors, rather than a single one. The prediction errors of these n predictors are measured first. These n prediction errors, relating to each cover pixel, are further employed into m new linear relations to generate m additional hybrid errors. Each optimal prediction error is then extracted from these $n+m$ errors in a manner so that these can be tracked back by the decoder during the de-embedment of the data bits. Simulation results confirm that the proposed scheme provides almost 10%–9233% higher embedding capacity depending on the texture contents of the cover image, while the image quality is improved compared with the competing ones.

1. Introduction

Since the last decade, the applications of covertly transmitting multimedia content have increased rapidly and massively. In many applications, the hiding of secret information in a cover media, more specifically in a cover image, is mostly performed by using either watermarking or steganography. The watermarking techniques are applied mainly into images and documents. In an image, this is used in both invisible and visible modes to protect the ownership and to declare the copyright respectively (Weng et al., 2013). The main objective of applying this technique is to maintain the integrity of the data, i.e., the cover medium, rather than securing the concealed information. The steganography, on the contrary, implants the secret bits into a media, say an image, so that concealed information are hid from all the sensing capabilities of the intruders (Provos, Honeyman, 2003, Brindha and Vennila, 2011; Chien-Chang and Tsai, 2011; Kamal, 2013; Kamal and Mahfuzul Islam, 2014). The image containing the hidden data is then termed as the 'stego image'.

* *Corresponding author.* Department of CSE, Jatiya Kabi Kazi Nazrul Islam University, Trishal, Mymensingh P.C. 2220, Bangladesh.
E-mail address: kamal@jkkniu.edu.bd (A.H.M. Kamal).
[1] Member, IEEE.

http://dx.doi.org/10.1016/j.jisa.2016.08.005
2214-2126/

Please cite this article in press as: A.H.M. Kamal, Mohammad M. Islam, Enhancing embedding capacity and stego image quality by employing multi predictors, Journal of Information Security and Applications (2016), doi: 10.1016/j.jisa.2016.08.005

The steganographic methodologies can be classified into irreversible and reversible processes based on their ability in reconstructing the cover image from the stego one at their data extraction phase. The irreversible techniques focus on extracting the implanted secrets only from the stego image (Böhme and Kirchner, 2013; Chao et al., 2009; Hong and Chen, 2012; Hong et al., 2012; Lee and Chen, 2010; Lee et al., 2014; Lin, 2011; Liu and Liao, 2008; Luo et al., 2011; Ulutas et al., 2011; Wang et al., 2011; Yang et al., 2010), whereas the reversible schemes retrieve both the embedded data and the cover image from the stego one (Chung et al., 2012; Fridrich et al., 2002; Gujjunoori and Amberker, 2013; Hong and Chen, 2010; Kamstra and Heijmans, 2005; Lu et al., 2009; Ong et al., 2014; Tai et al., 2009; Wang et al., 2013, Nguyen et al., 2015). The irreversible schemes are inapplicable when both the extracted information and the cover contents are equally important at the data extractor end for further processing. To manage the reversibility, the reversible schemes implant additional information during their data embedment process. Implantation of these additional bits decreases the original message embedding capacity, known as the pure embedding capacity, and increases some degrees of processing complexity. Nevertheless, these further increase both the security of the message and the robustness of the algorithm as one cannot retrieve and comprehend the secret information without realizing the meaning of these additional bits.

In the reversible data hiding arena, message bits are embedded either by shifting the histogram of the contents in the embedding space, e.g., spatial values, pixel differences and prediction errors, or by expanding the contents in the embedding space. Among these processes, the schemes which utilize prediction errors present both the higher embedding capacity and the better stego image quality because the sharper Laplacian-like distribution of the prediction errors in the prediction error histogram (PEH) allows more errors in the error domain to accept message bits rather than pixels in the spatial domain or the error residues in the difference domain. These also cause the pixels to be shifted by fewer amounts because the frequency of unaltered pixels increases along with the increment of embeddable pixels. Moreover, these schemes provide stronger security of the embedded data because of their undisclosed parameters like applied predictor, starting point of predictions in the image, number of associated pixels in the predictor and the other parameters of the predictor's own.

In the prediction error based reversible data embedment processes, a predictor first predicts either a single pixel (Hong, 2012) or a block of pixels (Hong and Chen, 2010) by exploiting the features of spatial association among the neighboring pixels of the cover image. Predictors are therefore classified as either 'single pixel predictor' or 'block pixel predictor'. Associated pixels, used to predict the target ones by the predictor, remain unchanged during the data hider process, also termed as the encoding process, for the benefits of extracting secret messages at the receiver. In both cases, subtracting the predicted values from their corresponding cover pixel values generates the prediction errors. Bit implantation process embeds data bits into two or more highest frequency errors. The single layer data embedment processes conceal data bits mainly into two highest appeared errors (Ou et al., 2013; Yang et al., 2013). The other errors are shifted by one unit to give space for the movement required for data concealment into these two embeddable errors. The multi-layers embedding schemes (Hong, 2012; Kamal and Islam, 2016b), on the other hand, implant data bits into more than two highest appeared errors. These increase the embedding capacity, but destroy the stego image quality notably. The applications, which are sensitive to stego image quality, thus prefer to embed data bits into single layer. The research presented in this paper aims to enhance both the embedding capacity and the stego image quality.

As a 'single pixel prediction' (SPP) scheme, Ou et al. (2013) proposed a scheme that predicts a pixel, say x, by using a partial differential equation (PDE). Four gradient differences, measured from x and each of its four neighbors on top, right, bottom and left, are employed in the PDE to approximate a value of x. Let x^1 be the primary estimation for x. The estimation process repeats for t times, $t > 0$, for better predicting the value of x. At each prediction step t, the process calculates four gradients of x^t, executes the PDE with new gradients to estimate the next step predicted value, x^{t+1} and updates x^t with x^{t+1} until the PDE goes to a stable state. A parameter, known as the 'stable parameter', controls the number of iterations. A static 'stable parameter' cannot predict all the pixel values, which are close to accurate. Dynamic valued 'stable parameter', on the contrary, reduces the pure embedding capacity, as the parameter information also needs to be implanted for the reason of assisting the decoding process at the receiver end. The scheme proposed by Yang et al. (2013) predicts values from a weighted average of its four neighbor pixels on the left, right, top and bottom. During the estimation of a pixel, the weights for vertical and horizontal neighbors are assigned by analyzing its vertical and horizontal gradient responses. For each pixel, the scheme applies Sobel and interpolation masks of size 5×5 in measuring these two gradient responses along its vertical and horizontal directions. Based on these responses, the scheme then allots more emphasis on either the vertical or the horizontal pixels by assigning more weights to them. The scheme, however, ignores the diagonal gradient responses and, thus, estimates poorly in many instances. Ma et al. (2015) presented a different scheme where they had employed multiple predictors so that an optimal one could be selected from the multiple predicted values. The scheme first predicts a pixel by each of the predictors separately and then measures the optimal predicted values verifying three situations — optimal value is a one of the predicted values if all the predictions are of the same worth; the minimum of the n-predicted values is an optimal one if the cover pixel is less than that minimum value; and finally, the maximum of the predicted values is an optimal one if the cover pixel is greater than that maximum value. The scheme avoids the cover pixels, whose values are within the range between the minimum and maximum predicted values, although such pixels are large in quantity. To reduce the distortions in the stego image, Chen et al. (2013) employed two asymmetric predictors; separately one for embedding bits at the right direction and another for embedding bits at the left direction into a single most appeared prediction error of the error histogram. The scheme only presents a new mechanism of embedding bits for twice rather than improving or proposing a new predictor. The scheme proposed by Wang et al. (2013) classifies the pixels into two groups: wall pixel (i.e., border pixels) and non-wall pixels. Interpolation errors are

Please cite this article in press as: A.H.M. Kamal, Mohammad M. Islam, Enhancing embedding capacity and stego image quality by employing multi predictors, Journal of Information Security and Applications (2016), doi: 10.1016/j.jisa.2016.08.005

computed from wall pixels to embed data. The non-wall pixels are first arranged by a defined traversing order. In this arrangement, a difference between a pixel and its immediate earlier traversed pixel is computed. These two pixels become always neighbors in the cover image. This way, all the differences are computed. The data bits are implanted into these computed pixel differences.

As a block pixel prediction (BPP) scheme, Tsai et al. (2009) first divided the image into non overlapping blocks. This scheme then estimated the entire pixels of a block from its center pixel. The embedding space is formed by measuring the error residues through subtracting the center pixel from all the other pixels in the block. The accuracy of the linear predictor used in this scheme, for predicting a block of pixels from a single reference value, is poor. Hong and Chen (2010) improved the prediction scheme by associating the center pixels of four neighbor blocks along with its own center pixel in their prediction rules. The process of estimating pixels in the block from several pixels improves the prediction accuracy as well as the embeddable prediction errors. For the purpose of reversibility, the entire block centers are remained unchanged. As the block size used in the scheme in Hong and Chen (2010) is 3×3, (1/8)th portion of the entire image represents the center of the blocks and none of them conceives any message bit. To solve the problem, Lu and Huang (2014) proposed a scheme, where a separate layer was made upon the original image by collecting the copies of these center pixels, and the same embedding process was carried out into the pixels in the upper layer. Kamal and Islam (2015) proved that the schemes presented in Hong and Chen (2010) and Lu and Huang (2014) cannot predict well in texture images when in a frequent manner deep valley or sharp hill exists around the working block. They proposed a new prediction scheme based on Euclidean distance to improve the prediction accuracy and the quantity of embeddable errors. In the scheme, a Euclidian distance between the predicting pixel and each of the associated center pixels is measured. The inverse of each Euclidean distance is used as the weighting factor of the respective associated center pixel during applying the weighted average rule. Another BPP based method proposed by Leung et al. (2013) improved the prediction accuracy through predicting block pixels by the corresponding block median value. The scheme generates the embedding space by subtracting the block median value from the block pixels. In a smaller sized block, this provides better prediction accuracy. The median value of each block is preserved to manage the reversibility in the decoder end. The prediction accuracy decreases when the size of the block is bigger. Kamal and Islam (2016a) presented a reversible scheme for improving the embedding capacity at the cost of intentional distortion of the cover image. I-Cheng et al. (2015) presented a scheme where data bits are implanted into the block truncation coded image by shifting the residual errors in the histogram. In the block truncation coding, at first the pixels of each block are categorized into two groups: 'above mean' and 'mean and below' based on a threshold equaling to block mean. All the pixels belong to the group of 'above mean' are quantized to a single value, say a. Similarly, all the pixels that belong to the group of 'mean and below' are also quantized to another single value, say b. A bitmap, say BM, is generated to track the pixels' origin, e.g., set 1 in BM for the pixels quantized with the value of a and set 0 for the pixels quantized with the value of b. These trio (a, b, BM) are used to code a block of pixels. The scheme collects one a from each block and arranges them in a plane. This plane is then divided into non-overlapping blocks of a defined size. The linear predictor predicts the entire pixels of a block by a single pixel, e.g., the pixel in mid-point in the block. The residues are computed by subtracting the predicted value from all other values in the block. At first, message bits are embedded through shifting the residual errors in the histogram. A deviation d is computed as $d = a - b$ for all the values of a and b. Message bits are embedded again by shifting the histogram of d. The b values are updated by subtracting stego d from stego a to preserve the block truncation coding property. Thus, a block can conceive at most two bits. Moreover, the scheme can be applicable in block truncated compressed image only.

In all the SPP and the BPP schemes, stated in the preceding sections, the quantity of the embedded bits, also known as the payload, depends on the frequencies of the two highest appeared prediction errors whereas the frequencies of these two errors depend on the accuracy of the predictor used. The message bits are implanted into the errors of either '–1' or '0' or into the two highest appeared errors, whatever these are, depending on the reviewed embedding algorithms. Experimentally it is observed that two highest appeared errors are generally '0' and '–1' and in several instances these are '0' and '1'. It is also investigated that when these two errors are '0' and '1', the frequencies of '–1' and '1' become nearly equal. That is why most of the stated schemes directly embed bits into the errors of '0' and '–1'. In all the schemes reviewed in the literature, at first, the positive and the negative valued non-embeddable errors shifted by 1 and –1, respectively, to prepare the required space for shifting the embeddable errors. These schemes embed message bit '0' into the embeddable errors without changing error values while the message bit '1' is implanted by shifting the errors by one unit. Thus, the shifting probabilities of embeddable and non-embeddable errors in the PEH are p and 1 respectively, where p states the probability of appearing a bit '1' in the message stream and $0 \le p \le 1$. The authors in various schemes tried to improve the prediction accuracy. Nevertheless, endeavors to improve the prediction accuracy and to increase the frequency of two embeddable errors, e.g., '0' and '–1', are not the same. In this paper, a better prediction policy employing n predictors is presented to enhance the frequencies of these two embeddable errors of '0' and '–1'. The proposed scheme first sequentially examines n prediction errors; if any of these n errors holds a value r, where $r \in \{-1, 0\}$, then r is considered as a final prediction error; otherwise it generates m new errors by forming m different linear relations with these n errors. The scheme then looks for an r inside these new m errors as well. Thus, the proposed scheme increases the frequencies of the two errors of –1 and 0. All the reviewed SPP based schemes (Chen et al., 2013; Ma et al., 2015; Ou et al., 2013; Yang et al., 2013) and BPP based schemes (Hong and Chen, 2010; I-Cheng et al., 2015; Kamal and Islam, 2015; Leung et al., 2013; Lu and Huang, 2014; Tsai et al., 2009) are experimented and compared with the scheme proposed in this paper. The simulation results demonstrate that the embedding capacity is improved notably compared with its competing schemes. Additionally, this scheme improves the stego image quality.

Please cite this article in press as: A.H.M. Kamal, Mohammad M. Islam, Enhancing embedding capacity and stego image quality by employing multi predictors, Journal of Information Security and Applications (2016), doi: 10.1016/j.jisa.2016.08.005

The remaining of the paper is organized in several sections. Section II explains the two predictor based schemes at first and again n predictors based scheme later in the following. In the meantime, this section also describes the data embedment and the data extraction process as well as the recovery policy of the cover image. The improvements on the two performance measuring parameters, i.e. embedding capacity and image quality, by the proposed scheme are delineated in Section III. A direction of our future works is provided in Section IV. Finally, few concluding remarks on this paper are noted in Section V.

2. Multi predictor based reversible data embedment scheme

The proposed reversible data embedment (RDE) scheme implants message bits into the prediction errors of –1 and 0. This scheme employs n predictors, say A_k for $1 \le k \le n$, in its prediction phase owing to increase the frequency of these two embeddable errors –1 and 0. Hence, this scheme is called multi predictor scheme and shortly as 'n-predictor' scheme, e.g., 2-predictor, and so on. Each of the n predictors, say the predictor A_k, separately predicts a cover pixel at (i, j) location of the image which is P_k. The P_k is a matrix of $P_{k,i,j}$ for all the values of i and j, i.e., all the values predicted for the cover image by using the predictor A_k. The prediction error for the pixel at location (i, j) by the predictor A_k, termed as $E_{k,i,j}$, is measured by subtracting the respective prediction value from the cover pixel, $I_{i,j}$, i.e., $E_{k,i,j} = I_{i,j} - P_{k,i,j}$. Let E_k be the matrix of all prediction errors $E_{k,i,j}$ for all values of i and j of the cover image measured for the predictor A_k, $1 \le k \le n$. For each pixel of the cover image, n prediction errors are calculated by using n predictors. These n prediction errors are further employed into m linear relations to yield m new values; hereafter these m values will be addressed as the hybrid errors. A total of $n+m$ errors are, therefore, produced by the proposed prediction scheme. The scheme sequentially checks $n+m$ errors to find either a –1 or a 0. If one of these two error values exists, the first encountered –1 or 0 is deemed as an optimal prediction error. Otherwise, the minimum of the m hybrid errors is regarded as the optimal prediction error. Following this principle, optimal prediction errors, say $e_{i,j}$, are obtained for all the pixels of the cover image. The encoder, i.e. data hider, keeps a track of the acting predictor ($AP_{i,j}$), i.e., optimal error provided predictor for each of the pixel at (i, j) location. The encoder embeds message bits into $e_{i,j}$ by a set of embedding rules. After passing the data embedment phase, these modified optimal errors are termed as the stego errors, $\tilde{e}_{i,j}$. If the amount of these modifications due to data embedment is $M_{i,j}$, then $\tilde{e}_{i,j} = e_{i,j} + M_{i,j}$. The encoder finally forms the stego image $S_{i,j}$ by adding these stego errors, $\tilde{e}_{i,j}$, with the corresponding $AP_{i,j}$ provided predicted values.

The embedding process works in that way so that each k^{th} predictor in the decoder end can predict the same value P_k from the stego image without any ambiguity. Like the encoder, the decoder also generates $n+m$ errors. The measurements of optimal stego errors are outlined in the following. The hidden message is extracted from these stego errors, and thereafter, the original prediction errors, like encoder produced prediction errors, are generated to retrieve the cover pixels using a set of rules.

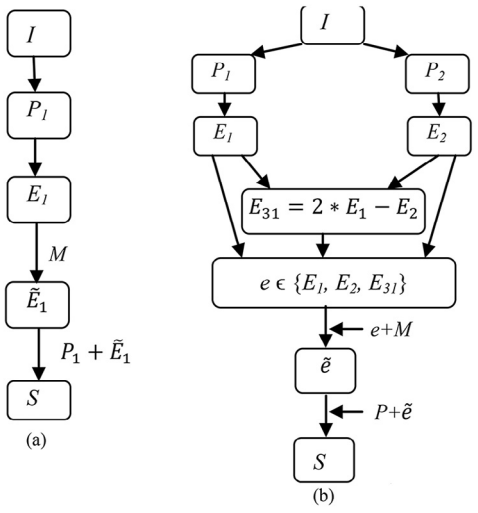

Fig. 1 – Single vs. two-predictor based RDE scheme.

Let M, e, $\tilde{e}$, I and S be the matrices of $M_{i,j}$, $e_{i,j}$, $\tilde{e}_{i,j}$, $I_{i,j}$ and $S_{i,j}$ respectively covering all the pixels of the entire cover image. For better realization of the proposed scheme, a single predictor based RDE scheme has been presented in Fig. 1a and a two-predictor based optimal error computation and data embedment process are detailed in Fig. 1b. Finally this optimal error computation based scheme has been generalized for n predictors in the following.

2.1. *Two-predictor based RDE scheme*

The conventional single predictor based RDE schemes, as shown in Fig. 1a, utilize only one predictor during their data embedment process. On the contrary, the proposed two-predictor based scheme applies two different predictors in its prediction phase. The scheme predicts each cover pixel separately by each of the predictors A_k, where $k \in \{1, 2\}$. The predicted values and the prediction errors of these two predictors A_1 and A_2 are managed by P_1, P_2, E_1 and E_2 respectively.

2.1.1. *Generating hybrid errors*

These two error matrices E_1 and E_2 are used to generate new errors, E_{3x}, termed as hybrid errors, from an expression $E_{3x} = \beta_{1,x}B_{1,x}E_1 + \beta_{2,x}B_{2,x}E_2$, where $x \in \{1, 2\}$; $\beta_{1,x}B_{1,x} + \beta_{2,x}B_{2,x} = 1$; both $\beta_{1,x}$ and $\beta_{2,x}$ belong to {–1, 1}; and $B_{1,x}$, $B_{2,x}$ are of integer value. Although $B_{1,x}$ and $B_{2,x}$ can hold any value maintaining the constraint of $\beta_{1,x}B_{1,x} + \beta_{2,x}B_{2,x} = 1$, for the process simplicity $B_{1,x}$ and $B_{2,x}$ are bounded here to hold one of the values of {1, 2}. Equations (1.1) and (1.2) are executed to produce two hybrid errors E_{31} and E_{32} (in the case of $B_{1,x}, B_{2,x} \in \{1, 2\}$).

$$E_{31} = 2 * E_1 - E_2 \tag{1.1}$$

$$E_{32} = 2 * E_2 - E_1 \tag{1.2}$$

A methodological difference between the two-predictor based embedding scheme and a single predictor based scheme

Please cite this article in press as: A.H.M. Kamal, Mohammad M. Islam, Enhancing embedding capacity and stego image quality by employing multi predictors, Journal of Information Security and Applications (2016), doi: 10.1016/j.jisa.2016.08.005

Algorithm 1: *CoverOptimalErrors*(E_1, E_2, E_{31}, E_{32})

1. If $E_1 = 0$ *or* $E_1 = -1$ *then*
2. $E_3 = E_1$ and $AP_{i,j}$=1
3. Else if $E_2 = 0$ *or* $E_2 = -1$ *then*
4. $E_3 = E_2$ and $AP_{i,j}$=2
5. Else if $E_{31} = 0$ *or* $E_{31} = -1$ *then*
6. $E_3 = E_{31}$ and $AP_{i,j}$=3
7. Else if $E_{32} = 0$ *or* $E_{32} = -1$ *then*
8. $E_3 = E_{32}$ and $AP_{i,j}$=4
9. Else
10. $E_3 = \min(E_{31}, E_{32})$
11. If $E_{31} \leq E_{32}$
12. $AP_{i,j}$=3
13. Else
14. $AP_{i,j}$=4
15. End if
16. End if

Fig. 2 – Generation of optimal prediction errors.

is depicted in Fig. 1a,b. Fig. 1b is a snapshot of the proposed embedding process that flows through Eq. (1.1).

2.1.2. *Generating optimal prediction errors*

Finally, each optimal prediction error E_3 (optimal error values are temporarily stored in this variable before saving to e) from the two prediction errors E_1 and E_2 and the two hybrid errors E_{31} and E_{32} is computed by Algorithm 1 of Fig. 2. A parameter AP keeps track of the optimal error presenting predictor individually for each of the pixel. This tracking information is usually a number, e.g., $AP_{i,j} = 1$ if $E_{1,i,j}$ is equal to –1 or 0, $AP_{i,j} = 2$ if $E_{2,i,j} \in \{-1, 0\}$ and so on. An illustration of the stated optimal prediction error generation process is provided in Example 1.

2.1.3. *Message embedment and stego image generation*

The computed optimal errors E_3 are assigned to a two dimensional matrix $e_{i,j}$, i.e. $e_{i,j} = E_{3,i,j}$. All the message bits are then embedded into $e_{i,j}$ by Eq. (2) in the encoder side. After the concealment of information, the modified errors, $\tilde{e}_{i,j}$, are assigned to $\tilde{E}_{3,i,j}$, i.e., $\tilde{E}_{3,i,j} = \tilde{e}_{i,j}$. As a final step in the encoder end, Eq. (3) generates the stego image S.

$$\tilde{e}_{i,j} = \begin{cases} e_{i,j}\omega s & \text{if } e_{i,j} = 0 \text{ or } e_{i,j} = -1 \\ e_{i,j}\omega 1 & \text{if } e_{i,j} > 0 \text{ or } e_{i,j} < -1 \end{cases} \quad (2)$$

where $\omega = sign\_of(e_{i,j})$

$$S_{i,j} = \begin{cases} P_{1,i,j} + \tilde{E}_{3,i,j} & \text{if } AP_{i,j} = 1 \quad (3.1) \\ P_{2,i,j} + \tilde{E}_{3,i,j} & \text{if } AP_{i,j} = 2 \quad (3.2) \\ P_{1,i,j} + \tilde{E}_{3,i,j} - E_{1,i,j} + E_{2,i,j} & \text{if } AP_{i,j} = 3 \quad (3.3) \\ P_{2,i,j} + \tilde{E}_{3,i,j} + E_{1,i,j} - E_{2,i,j} & \text{if } AP_{i,j} = 4 \quad (3.4) \end{cases} \quad (3)$$

The pixels associated in the prediction rules remained unchanged. The process of the data embedment and the stego image generation is explained in Example 2.

Example 1.. Generating optimal prediction errors.. *Assume an image block as shown in Fig. 3a. Let the values of the center pixels of four of its neighbor blocks situated on top, right, bottom and left be 53, 54, 53 and 52 respectively. The predicted values computed by Tsai et al. (2009) and Hong and Chen (2010) schemes are tabulated in Fig. 3b,c respectively. The respective prediction errors E_1 and E_2 are tabulated in Fig. 3d,e correspondingly.*

Hybrid prediction errors E_{31} and E_{32} are measured applying Eqs. (1.1) and (1.2) and these are tabulated in Fig. 3f,g respectively. Finally, Algorithm 1 of Fig. 2 computes the optimal errors E_3. Fig. 3h demonstrates the generated optimal errors. Fig. 3i lists the corresponding applied predictors. Each predictor generates 8 errors. Among these 8 errors, the number of embeddable errors, i.e., –1 and 0, is 38% (3/8) in E_1, 63% (5/8) in E_2, 13% (1/8) in E_{31}, 75% (6/8) in E_{32} and 100% (8/8) in E_3. The improvement in the quantity of embeddable errors in the calculated optimal errors is 62% and 37% regarding E_1 and E_2 respectively.

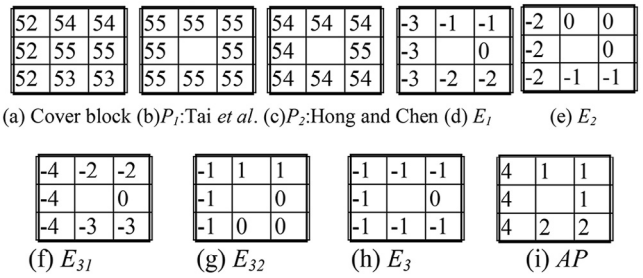

Fig. 3 – Generating optimal prediction errors in the two-predictor scheme. (a) is an instance of a cover image block. (b) and (c) are the results of the predictors which are proposed by Tsai et al. and Hong and Chen. Their prediction errors are shown in (d) and (e). (f) and (g) tabulate the hybrid errors. Finally, (h) and (i) state the optimal errors and list of applied predictors.

Example 2. The process of the data embedment into the optimal errors and the stego image generation.. *The E_3 computed in Example 1 are copied into $e_{i,j}$ in Fig. 4a. Let a chunk of the message stream that is to be embedded be '11101001'. Equation (2) implants these message bits into $e_{i,j}$. Fig. 4b demonstrates these stego errors $\tilde{e}_{i,j}$. The data embedment process is started from the upper left corner and the scheme embeds bits into the errors row-by-row. The components of Eq. (3), e.g. (3.1), (3.2), (3.3) and (3.4), to which the AP matches during the stego block generation, are noted in Fig. 4f. The computed stego block is depicted in Fig. 4g. For the convenience of stego image generation, an instance of the AP, P_1, P_2, E_1 and E_2 of Example 1 is copied here in Fig. 4c–g respectively.*

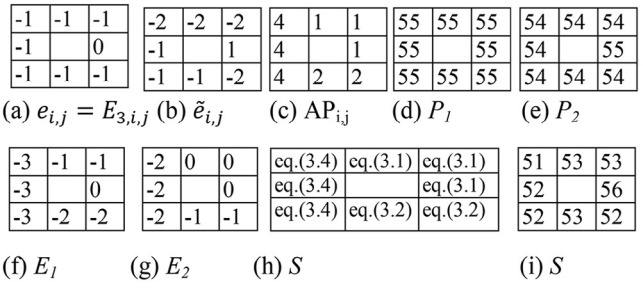

Fig. 4 – The process of data embedment into the optimal errors and the stego image generation. (a)–(g) aid in the data embedment process while (f) provides the stego image which is (g).

Please cite this article in press as: A.H.M. Kamal, Mohammad M. Islam, Enhancing embedding capacity and stego image quality by employing multi predictors, Journal of Information Security and Applications (2016), doi: 10.1016/j.jisa.2016.08.005

2.1.4. *Message extraction and cover image reconstruction*

The decoder applies the same n predictors in the stego image to predict stego pixels separately. Let these predicted values be P_k^d. The encoder did not change the pixels which took part in the prediction rules. This implies that these P_k^d and P_k are the same, i.e. $P_k == P_k^d$ for all k. The scheme measures the stego prediction errors $\tilde{E}_{k,i,j}$ by $\tilde{E}_{k,i,j} = S_{i,j} - P_{k,i,j}^d$, e.g. $\tilde{E}_{1,i,j} = S_{i,j} - P_{1,i,j}^d$ and $\tilde{E}_{2,i,j} = S_{i,j} - P_{2,i,j}^d$. The stego hybrid errors $\tilde{E}_{31}$ and $\tilde{E}_{32}$ are generated by Eqs. (4.1) and (4.2) respectively.

$$\left.\begin{aligned}\tilde{E}_{31} &= 2 * \tilde{E}_1 - \tilde{E}_2 \quad (4.1)\\ \tilde{E}_{32} &= 2 * \tilde{E}_2 - \tilde{E}_1 \quad (4.2)\end{aligned}\right\} \tag{4}$$

The *AP* and the stego optimal errors $\tilde{E}_3$ are generated by the decoder. This generation process is depicted in the flowchart of Fig. 6. This figure states the process of generating the *AP* and the optimal stego errors for n predictors rather than two. Nevertheless, this is fully realizable for $n = 2$. In this process, at first, the decoder collects the entire stego and hybrid errors which are generated by it for a single stego pixel. The decoder, next, checks the entire error sequentially to find a first encountered error which is either –1 or 0. If the decoder finds such an error, this is regarded as an optimal stego error and the corresponding acting predictor is assigned to $AP_{i,j}$. Otherwise, the similar way, the decoder tries to find an error with the value of –2 or 1 and then saves it as an optimal stego error and the acting predictor to $AP_{i,j}$. If the decoder fails again, the decoder collect the minimum valued error from the hybrid errors as an optimal stego error and assigns the corresponding acting predictor to $AP_{i,j}$. Thus, the decoder calculates the optimal stego errors, $\tilde{E}_3$, and the full *AP* for the entire pixels.

Assigning these optimal stego errors $\tilde{E}_3$ into $\tilde{e}_{i,j}$, Eqs. (5) and (6) are executed to extract each message bit s and the optimal cover error $e_{i,j}$ respectively. Finally, Eq. (7) constructs the cover image I.

$$s = \begin{cases} 0 & \text{if } \tilde{e}_{i,j} = 0 \text{ or } \tilde{e}_{i,j} = -1 \\ 1 & \text{if } \tilde{e}_{i,j} = 1 \text{ or } \tilde{e}_{i,j} = -2 \end{cases} \tag{5}$$

$$e_{i,j} = \begin{cases} \tilde{e}_{i,j} \odot 1 & \text{if } \tilde{e}_{i,j} > H_p \text{ or } \tilde{e}_{i,j} < H_n \\ \tilde{e}_{i,j} & \text{Otherwise} \end{cases} \tag{6}$$

where $\odot = sign\_of(-1 * \tilde{e}_{i,j})$, $H_p = 0$ and $H_n = -1$

$$I_{i,j} = \begin{cases} P_1 + e_{i,j} & \text{if } AP_{i,j} = 1 \quad (7.1) \\ P_2 + e_{i,j} & \text{if } AP_{i,j} = 2 \quad (7.2) \\ P_1 + e_{i,j} - \tilde{E}_1 + \tilde{E}_2 & \text{if } AP_{i,j} = 3 \quad (7.3) \\ P_2 + e_{i,j} + \tilde{E}_1 - \tilde{E}_2 & \text{if } AP_{i,j} = 4 \quad (7.4) \end{cases} \tag{7}$$

An illustration of message extraction and cover image reconstruction is provided in Example 3.

Example 3.. Message extraction and cover image reconstruction from the stego image.. *The stego block is re-printed in Fig. 5a from Example 2. The same predictors A_1 and A_2 are again applied in the stego block. Figs. 5b and 6d list the predicted values P_1 and P_2 respectively. The corresponding stego prediction errors $\tilde{E}_1$ and $\tilde{E}_2$ are shown in Figs. 5c and 6e respectively. Equations (4.1) and (4.2) generate the stego hybrid errors $\tilde{E}_{31}$ and $\tilde{E}_{32}$ which are depicted in Figs. 5f and 6g respectively. Fig. 6 provides the optimal stego errors $\tilde{E}_3$ and the list of AP. All the optimal stego errors and list of the applied predictor are demonstrated in Fig. 5h and 6i respectively. Equation (5) will extract the message '11101001', as shown in Fig. 5k, from $\tilde{E}_3$ of Fig. 5i. The original stego errors computed by Eq. (6) are tabulated in Fig. 5j. The components of Eq. (7), i.e. (7.1) to (7.4), which are applied in each cell during the stego image generation, are shown in Fig. 5l. The application of these components of Eq. (7) reforms the cover image block, as shown in Fig. 5m.*

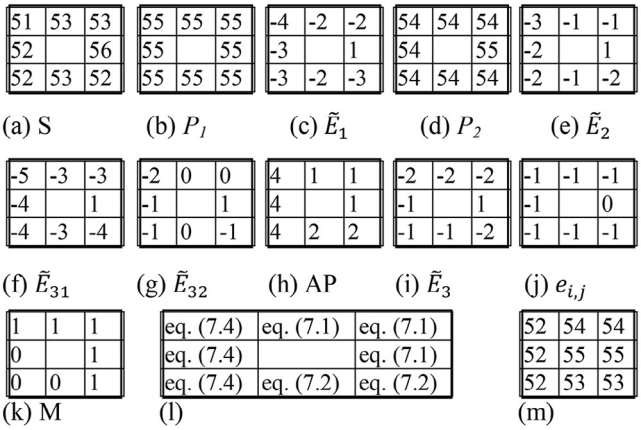

Fig. 5 – Optimal error generations, message extractions and cover reconstructions. Figures in (a), (b) and (d) represent the stego image block, predicted values by Tsai et al.'s and predicted values by Hong. (c) and (e)–(h) are used to compute the stego optimal errors in (i). (j) and (k) are to display recovered prediction errors and the extracted message respectively. (l) and (m) are used to reconstruct the cover block.

2.2. *Multi-predictor based RDE scheme*

In the n-predictor scheme, the hybrid prediction errors are generalized by Eq. (8).

$$E_{n+1,m} = \beta_{1,m}B_{1,m}E_{1,m} + \ldots\ldots + \beta_{n,m}B_{n,m}E_{n,m} \tag{8}$$

where $\beta_{1,m}B_{1,m} + \beta_{2,m}B_{2,m} + \ldots\ldots + \beta_{n,m}B_{n,m} = 1$, each of the $\{\beta_{1,m}, \beta_{2,m} \ldots\ldots\ldots \beta_{n,m}\}$ can hold a value from {1, –1} and m is the number of possible expressions represented by Eq. (8). Primarily 1 is assigned to all the $B_{k,m}$, for $k = 1$ to n. If n is an even number then in each m expression, only one $B_{k,m}$ will be updated by the value of 2.

One can observe in Eq. (4.1) that $B_{1,1} = 2$, $\beta_{1,1} = 1$, $B_{2,1} = 1$ and $\beta_{2,1} = -1$ and in Eq. (4.2) that $B_{1,2} = 1$, $\beta_{1,2} = -1$, $B_{2,2} = 2$ and $\beta_{2,2} = 1$. A list of possible $E_{n+1,m}$ for 3, 4 and 5 predictors, i.e. $n = 3$, $n = 4$ and $n = 5$, is shown in Table 1.

Algorithm 1 of Fig. 2 employs all of these $E_1, E_2, \ldots\ldots\ldots, E_n$ and $E_{n+1,m}$ to measure the optimal errors E_{n+1}. Note that there, E_1, E_2, E_{31} and E_{32} are checked sequentially. To do the same, a slight modification is done in the code fragment of Algorithm 1. Like 2-predictor method, n-predictor scheme serially checks n prediction errors, i.e. $E_1, E_2, \ldots\ldots, E_n$, and m hybrid prediction errors, i.e. $E_{n+1,m}$ to find the optimal error and then this records the respective *AP*. After computing all the optimal errors and AP,

Please cite this article in press as: A.H.M. Kamal, Mohammad M. Islam, Enhancing embedding capacity and stego image quality by employing multi predictors, Journal of Information Security and Applications (2016), doi: 10.1016/j.jisa.2016.08.005

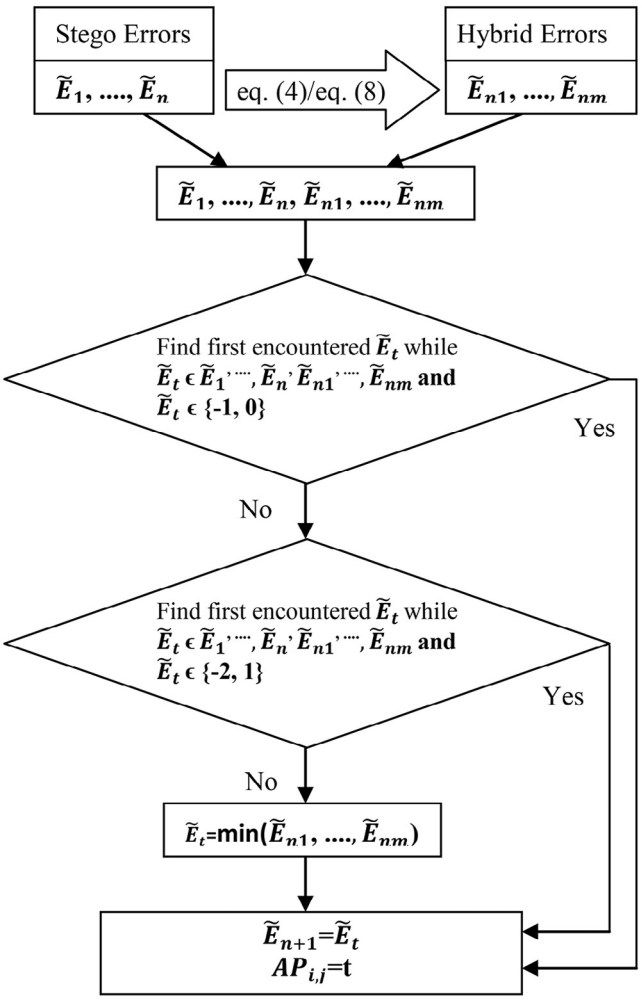

Fig. 6 – Generation of optimal prediction errors and *AP* list.

this assigns E_{n+1} to $e_{i,j}$. The embedding is done into the errors of $e_{i,j}$ by Eq. (2). The stego errors $\tilde{e}_{i,j}$ constructed by Eq. (2) are copied to $\tilde{E}_{n+1}$. Finally, Eq. (9) produces the stego image.

$$S_{i,j} = \begin{cases} P_{A_{i,j}} + \tilde{E}_{n+1} & \text{if } AP_{i,j} \le n \\ I_{i,j} + \tilde{E}_{n+1} - E_{n+1} & \text{otherwise} \end{cases} \quad (9)$$

Table 1 – Possible expression for hybrid errors $E_{n+1,m}$.

m	Values of $E_{n+1,m}$ for		
	n = 3	n = 4	n = 5
1	$E_1 - E_2 + E_3$	$2E_1 + E_2 - E_3 - E_4$	$E_1 + E_2 + E_3 - E_4 - E_5$
2	$E_1 + E_2 - E_3$	$E_1 + 2E_2 - E_3 - E_4$	$E_1 + E_2 - E_3 + E_4 - E_5$
3	$-E_1 + E_2 + E_3$	$2E_1 - E_2 + E_3 - E_4$	$E_1 + E_2 - E_3 - E_4 + E_5$
4		$E_1 - E_2 + 2E_3 - E_4$	$E_1 - E_2 + E_3 + E_4 - E_5$
5		$2E_1 - E_2 - E_3 + E_4$	$E_1 - E_2 + E_3 - E_4 + E_5$
6		$E_1 - E_2$-$E_3 + 2E_4$	$E_1 - E_2 - E_3 + E_4 + E_5$
7		$-E_1 - E_2 + 2E_3 + E_4$	$-E_1 + E_2 + E_3 + E_4 - E_5$
8		$-E_1 - E_2 + E_3 + 2E_4$	$-E_1 + E_2 + E_3 - E_4 + E_5$
9		$-E_1 + 2E_2 + E_3 - E_4$	$-E_1 - E_2 + E_3 + E_4 + E_5$
10		$-E_1 + E_2 + 2E_3 - E_4$	$-E_1 + E_2 - E_3 + E_4 + E_5$
11		$-E_1 + 2E_2 - E_3 + E_4$	
12		$-E_1 + E_2 - E_3 + 2E_4$	

In the decoder end, the data extractor generates n prediction errors $\tilde{E}_1, \ldots, \tilde{E}_n$ and m hybrid errors $\tilde{E}_{n+1}, \ldots, \tilde{E}_{n+m}$ for each of the processing stego pixels. Like the 2-predictor method, the decoder computes *AP* and the optimal stego errors $\tilde{E}_{n+1}$.

The optimal error generation process is depicted in Fig. 6. The functionality of that flowchart is explained above. Let us explain it by an example. Assume the prediction errors of E_1, E_2 and E_3 of three separate predictors are –2, –1 and 0 respectively. The hybrid errors of E_{41}, E_{42} and E_{43} computed from the expressions stated in Table 1 are –1, –3 and 1 respectively. In the encoder end, Algorithm 1 of Fig. 2 generates an optimal error $E_4 = -1$ and $AP = 2$. If '0' bit is embedded into this error, stego error $\tilde{E}_4$ will be –1, i.e., no changed. The decoder is blind about the value of the optimal error $\tilde{E}_4$, the *AP* and the embedded bit. Nevertheless, the decoder is able to compute $\tilde{E}_1 = -2$, $\tilde{E}_2 = -1$ and $\tilde{E}_3 = 0$ and then $\tilde{E}_{41} = -1$, $\tilde{E}_{42} = -3$ and $\tilde{E}_{43} = 1$. Once the hybrid errors are placed after the n stego errors, these $\tilde{E}_{41}$, $\tilde{E}_{42}$ and $\tilde{E}_{43}$ will be regarded as $\tilde{E}_4$, $\tilde{E}_5$ and $\tilde{E}_6$. In that case, $\tilde{E}_2$ is the first encountered one that holds either1, i.e., $\tilde{E}_2 \in \{-1, 0\}$. Hence, the optimal stego error is $\tilde{E}_2$ which is –1 and the respective $AP_{i,j}$ is 2. Equations (5) and (6) extract the message bit '0' and reconstruct the error to –1 respectively.

In the n-predictor scheme Eq. (5) extracts the embedded message bits from $\tilde{E}_{n+1}$. Equation (6) reconstructs $e_{i,j}$ from these optimal stego errors. Finally, Eq. (10) constructs the cover image in the n-predictor scheme.

$$I_{i,j} = \begin{cases} P_k + e_{i,j} & \text{if } AP_{i,j} \le n \\ S_{i,j} + e_{i,j} - \tilde{E}_{n+1} & \text{otherwise} \end{cases} \quad (10)$$

3. Result analysis

The main objective of the proposed research work is to increase the embedding capacity of the prediction error based reversible data embedment schemes. In the meantime, it enhances the quality of the stego image. The experiments are conducted on 50 USC-SIPI texture images (Signal and Image Processing Institute, University of Southern California, USA, 2016a, <http://sipi.usc.edu/database/database.php?volume=textures>), 50 USC-SIPI standard images (Signal and Image Processing Institute, University of Southern California, USA, 2016b, <http://sipi.usc.edu/database/database.php?volume=misc>), 5000 CalTech101 images (Fei-Fei et al., 2004), 50 images with natural scene (National History Museum Public Library, UK, 2016, <http://piclib.nhm.ac.uk/>) and 50 CRISP's satellite images (Centre for Remote Imaging, Sensing and Processing, National University of Singapore, 2016, <https://crisp.nus.edu.sg/coverage/S_NPPindex.php>) in MATLAB. All these image datasets are utilized during the experiment of both the single pixel prediction and block pixel prediction based schemes. As SPP based schemes, the predictors of Hong (2012), Tai et al. (2009), Yang et al. (2013), Ma et al. (2015) and Chen et al. (2013) are tested and compared with the proposed n-predictor policies. The predictors of Tsai et al. (2009), Hong and Chen (2010), Lu and Huang (2014), Kamal and Islam (2015), Leung et al. (2013) and I-Cheng et al. (2015) are employed in exploiting the BPP based schemes. Before applying the Chang et al.'s scheme,

Please cite this article in press as: A.H.M. Kamal, Mohammad M. Islam, Enhancing embedding capacity and stego image quality by employing multi predictors, Journal of Information Security and Applications (2016), doi: 10.1016/j.jisa.2016.08.005

Table 2 – An interpretation of the legends used in Figs. 7–10.

Sr.	Legend	Meaning (Scheme of)
1	Tai	Tai et al. (2009); Tai 2009
2	Wien	Hong (2012)
3	Weijen	Yang et al. (2013)
4	Xiao2	Ma et al. (2015) with two predictors
5	Xiao3	Ma et al. (2015) with three predictors
6	Xiao4	Ma et al. (2015) with four predictors
7	Kamal	Kamal and Islam (2015)
8	Leung	Leung et al. (2013)
9	Wien	Hong and Chen (2010)
10	Tsai	Tsai et al. (2009)
11	Mid	Chen et al. (2013)
12	Truncation	I-Cheng et al. (2015)
13	P2	Hong (2012) and (Yang et al. (2013)
14	P3	Combined Hong (2012), Yang et al. (2013), and Tai et al. (2009)
15	P4	Combined Hong (2012), Yang et al. (2013), Tai et al. (2009), and Xiao2
16	P5	Combined (Hong, 2012) (Yang et al., 2013), (Tai et al., 2009), Xiao2 and Xiao3
17	P2:KL	Combined Kamal and Islam (2015) and Leung et al. (2013)
18	P3:KLW	Combined Kamal and Islam (2015), Leung et al. (2013), and Hong and Chen (2010)
19	P4:KLWT	Combined Kamal and Islam (2015), Leung et al. (2013), Hong and Chen (2010), and Tsai et al. (2009)
20	P5:KLWTM	Combined Kamal and Islam (2015), Leung et al. (2013), Hong and Chen (2010), Tsai et al. (2009), and Mid

the image pixels are converted to truncation coded values in our experiments.

In both the prediction categories, i.e., SPP and BPP, the proposed *n*-predictor scheme dictates the others by all the performance measuring parameters like payload, PSNR and Structural Similarity Index Matrix (SSIM). As a proposed *n*-predictor scheme, the 2-predictor, 3-predictor, 4-predictor and 5-predictor are analyzed. Generally, '*n*-predictor' will be used in a sentence in this article to address it as a singular collective noun. On the other hand, the phrase '*n*-predictor policies' will act as plural collective noun. In the demonstration, the performance measuring values are plotted along the y axis for the experimented images. For a better depiction, only the results of 15th to 45th images are presented in the figures in the following. Each legend in the figures represents a scheme. The meaning of the legends is tabulated in Table 2. These 20 schemes, as listed in Table 2, are separately experimented and the results are compared in this article.

3.1. *Analysis on the performance of the predictors*

The target of the proposed predictor is to increase the quantity of the embeddable prediction errors i.e., –1 and 0. Taking the best of all, the *n*-predictor scheme enhances the quantity of these two embeddable errors. Fig. 7 depicts two prediction error histograms which are drawn by grouping the predictors of SPP and BPP techniques in Fig. 7(a) and (b) respectively. As a sample, only the 3-predictor is demonstrated in this figure. In both cases, i.e., in SPP and BPP, 3-predictor scheme noticeably dominates the others by increasing the frequencies of the several highest appeared errors. The *n*-predictor scheme produces the highest frequency for the '0' valued error. The scenario is the same while comparing the frequencies of '–1' valued errors. Hence, the summation of these two embeddable errors is a lot more than the others. By improving the frequencies of the errors of –1 and 0, the *n*-predictor scheme enhances the prediction accuracy as well. To test the prediction accuracy, pre-

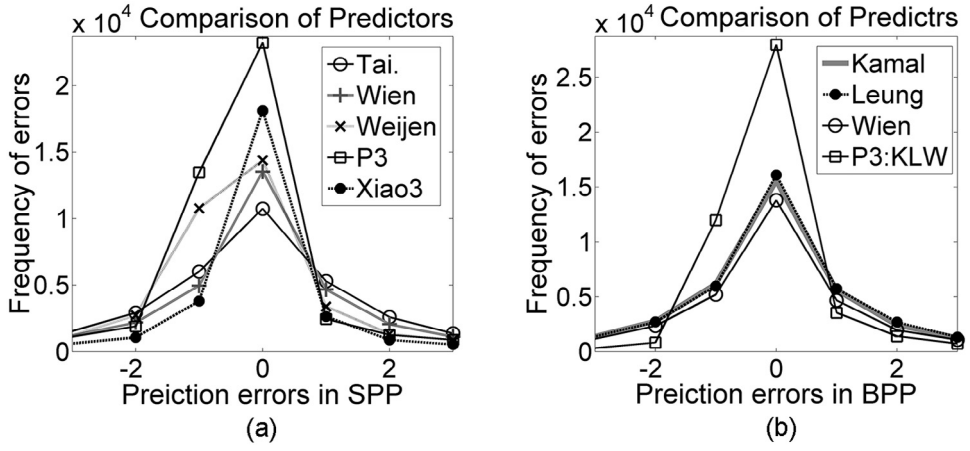

Fig. 7 – Comparison of prediction errors in SPP and BPP techniques.

Please cite this article in press as: A.H.M. Kamal, Mohammad M. Islam, Enhancing embedding capacity and stego image quality by employing multi predictors, Journal of Information Security and Applications (2016), doi: 10.1016/j.jisa.2016.08.005

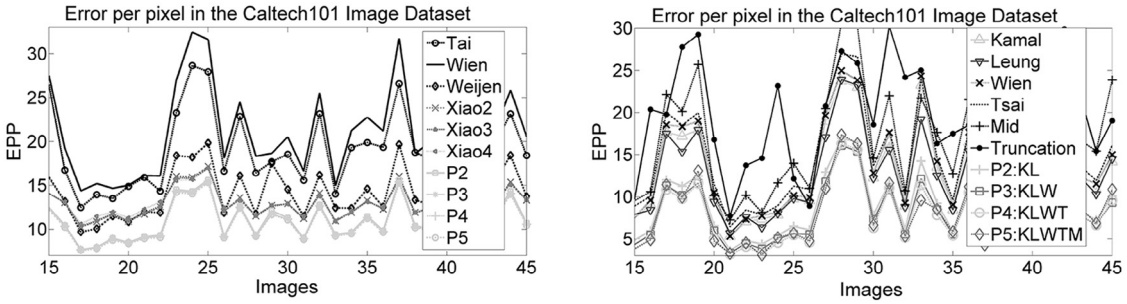

(a) Prediction errors per pixel in the SPP based predictors.

(b) Prediction errors per pixel in the BPP based predictors.

Fig. 8 – A comparison of EPP among the schemes.

diction errors per predicting pixel (EPP) are measured. The values of the EPPs in the n-predictor policies are smaller than their competing schemes, as shown in Fig. 8a,b.

3.2. *Analysis on the embedding payload*

The total number of embedded bits, i.e., payload, by each scheme is measured in each image separately. Block or pixel skipping criteria (Hong, 2012; Hong and Chen, 2010; Kamal and Islam, 2015; Leung et al., 2013) are omitted to allow the schemes to embed data bits at their maximum capabilities. The payloads, which are obtained in the images of CalTech101 dataset, are delineated in Fig. 9. Fig. 9a illustrates that SPP based multi-predictor schemes like Xiaoxiao et al.'s (e.g., Xiao2, Xiao3, Xiao4) and proposed n-predictor policies (e.g., P1, P2, . . ., Pn) demonstrate superior payloads than all the single predictor based schemes, e.g. Tai, Wien, Weijen. Furthermore, the n-predictor policy shows the optimal value for payload at a significant mark. This also investigated that the amount of payload rises for the use of more predictors, i.e., PL(P2, I) > PL(P3, I) > PL(P4, I) > PL(P5, I), where PL(X, I) represents the achieved payloads in the image I by the X scheme. Similarly, Fig. 9b exhibits the distinguishable performance of the proposed n-predictor policy over all the other BPP based schemes. These two figures prove that the n-predictor scheme outperforms in all the ways.

Embedding gains are analyzed to figure out the rate of improvement of n-predictor policy over the competing schemes. The embedding gains of the proposed n-predictor scheme over the reviewed methodologies in each image I are measured in percentage by Eq. (11).

$$\text{Embedding } Gain(I) = \frac{PL(X,I) - PL(Y,I)}{PL(Y,I)} 100\% \tag{11}$$

where $X \in$ {'P2', 'P3', 'P4', 'P5', 'P2: KL', 'P3: KLW', 'P4: KLWT', 'P5: KLWTM'}, and $Y \in$ {'*Tai*', '*Wien*', '*Weijen*', '*Xiao2*', '*Xiao3*', '*Xiao4*', '*Kamal*', '*Leung*', '*Wien*', '*Tsai*', '*Mid*', '*Truncation*'}.

As a sample, the minimum and the maximum gains of the 4-predictor policy are tabulated in Tables 3 and 4 only for the CalTech101 image dataset. All the minimum gains are of positive value. Several of the maximum gains are praiseworthy notable; even, these are some multiples of their competing schemes. The proposed scheme achieves highest gains over the embedding into the truncated image for two reasons. First, the data hider implants at best two bits per block in a truncated image because the truncated image contains only two quantized encoded integer values in each block and, therefore, the applied linear predictor generates only two error residues in a block. Second, the linear predictor operates on a group of pixels while the pixels are collected from the separate blocks in the truncated image. These pixels, which come from separate places, are more uncorrelated. The applied linear predictor then distributes its error residues over the error space more evenly rather than concentrating the majority of errors to a few values.

3.3. *Analysis on the image quality*

The data embedment scheme alters the visual, the structural and the statistical information in the stego image regarding its cover image. The level of modification is estimated by either

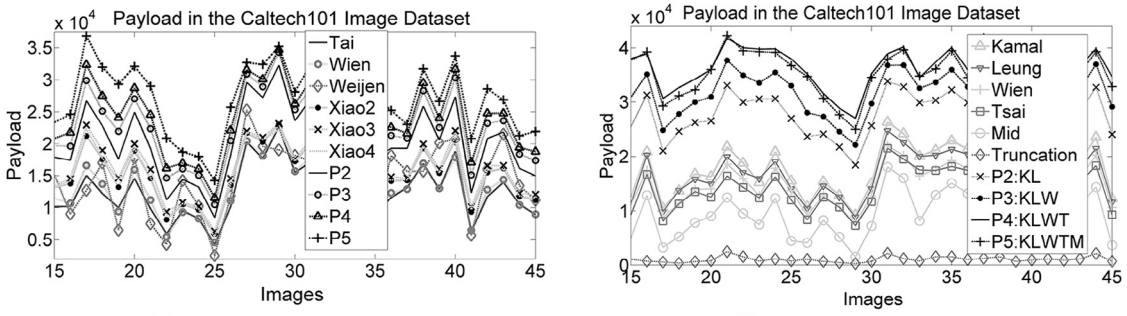

(a) Payload in the SPP based schemes.

(b) Payload in the BPP based schemes.

Fig. 9 – Comparison of payloads among the schemes.

Please cite this article in press as: A.H.M. Kamal, Mohammad M. Islam, Enhancing embedding capacity and stego image quality by employing multi predictors, Journal of Information Security and Applications (2016), doi: 10.1016/j.jisa.2016.08.005

Table 3 – Embedding Gains of 4-predictor policy over SPP based schemes in CalTech101 image dataset.

Gain of 3-predictor over the ↓	CalTech101	
	Min	Max
Tai	25	152
Wien	21	143
Weijen	19	519
Xiao2	21	71
Xiao3	18	56
Xiao4	19	83

pixel difference measurement process or human visual based measurement processes. Two common mechanisms of pixel difference measurements are mean-square-errors (MSE) and peak-signal-to-noise-ratio (PSNR). On the other hand, two widespread human visual based measurement policies are structural similarity index (SSIM) and universal image quality index (UIQI). In this subsection, the image quality is measured and compared in terms of the PSNR and the SSIM values.

Table 4 – Embedding Gains of 4-predictor policy over BPP based schemes in CalTech101 image dataset.

Gain of 3-predictor over the ↓	CalTech101	
	Min	Max
Kamal	27	199
Leung	19	181
Wien	35	211
Tsai	27	226
Mid	54	1276
Truncation	1351	8349

3.3.1. *Analysis on PSNR values*

The PSNR of a stego image S of size hxw, generated by embedding data bits into a cover image I of same size, is measured by Eq. (12).

$$PSNR = 10\log\frac{255^2}{MSE} \tag{12}$$

where

$$MSE = \frac{\sum_{i=1}^{m}\sum_{j=1}^{n}(S_{i,j} - I_{i,j})^2}{hxw} + \epsilon$$

Here, $\epsilon = 0.65 \times 10^{-5}$ and this is added to measure the 100 dBm of PSNR while comparing two same images. The PSNR loss in each image due to data embedment is computed by Eq. (13)

$$PSNR\_LOSS = 100 - PSNR \tag{13}$$

Fig. 10a,b depicts the number of the implanted bits per PSNR losses in the CalTech101 image dataset as a clipped portion of the whole dataset. The figure clearly depicts that the n-predictor policies implant more number of bits for the same level of PSNR losses than all the other competing schemes. This also investigated that the amount of payload per PSNR_LOSS increases for each higher value of n in the n-predictor scheme. Fig. 10c,d also demonstrates that all the n-predictor policies provide higher PSNR during the same amount of data embedment. Thus, Fig. 10 establishes that the proposed scheme maintains better image quality by PSNR value.

3.3.2. *Analysis on SSIM values*

SSIM (Zhou Wang, 2002) was proposed as an improvement of UIQI. In this measurement, the structural similarities between

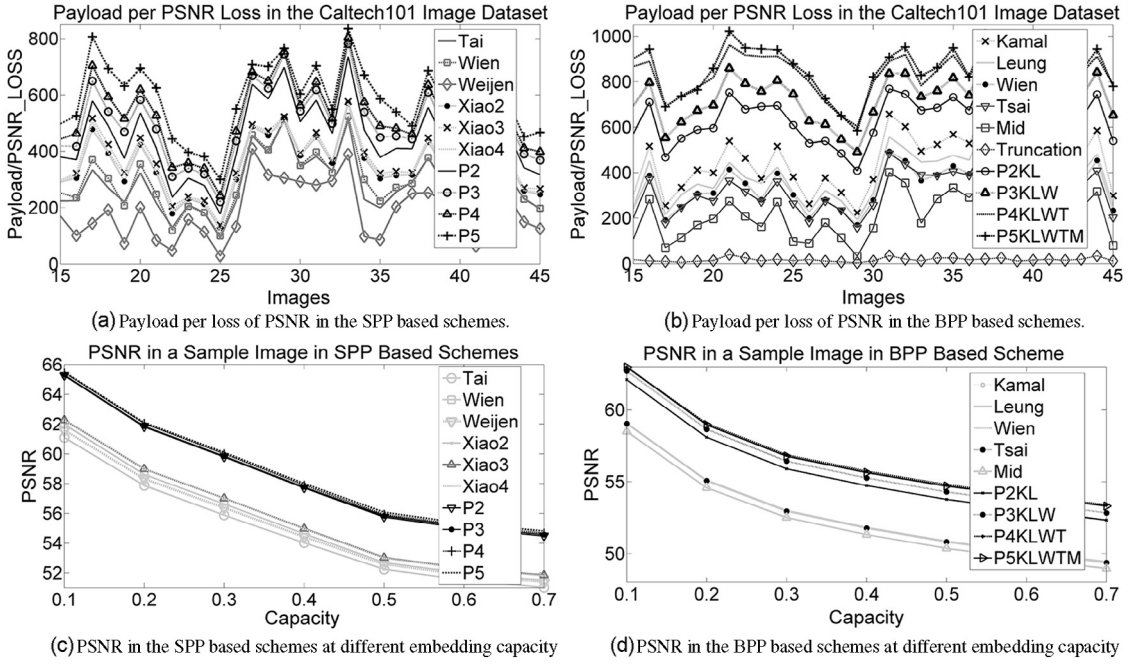

(a) Payload per loss of PSNR in the SPP based schemes.

(b) Payload per loss of PSNR in the BPP based schemes.

(c) PSNR in the SPP based schemes at different embedding capacity

(d) PSNR in the BPP based schemes at different embedding capacity

Fig. 10 – Comparison of embedding efficiency regarding the PSNR values among the schemes.

Please cite this article in press as: A.H.M. Kamal, Mohammad M. Islam, Enhancing embedding capacity and stego image quality by employing multi predictors, Journal of Information Security and Applications (2016), doi: 10.1016/j.jisa.2016.08.005

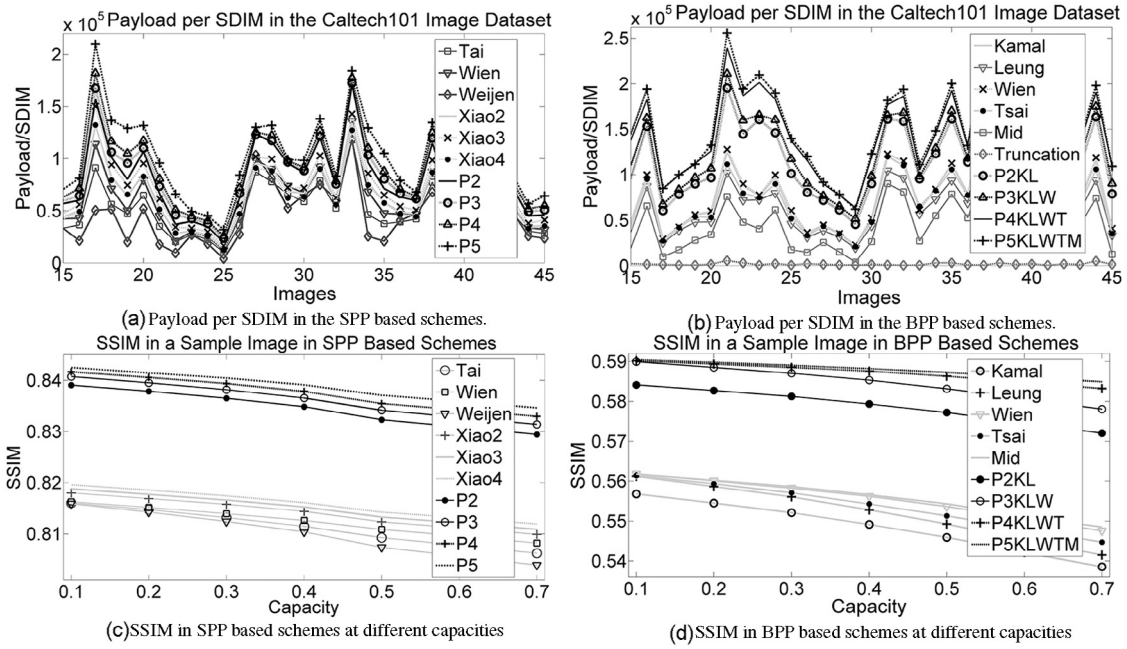

Fig. 11 – Comparison of embedding efficiency regarding the structural similarity index values among the schemes.

two images are represented as a single numerical value. First, both the cover and the stego images are divided by $d \times d$ sized blocks, say 3×3. Second, a mean and a variance are computed from each block in cover and stego images; say, these are μ_C, μ_S, σ_C^2 and σ_S^2 respectively. One covariance σ_{CS}^2 between the cover and the stego block is measured. Next, the SSIM between the i^{th} blocks of the cover and the stego image is computed by Eq. (14).

$$SSIM_i(I,S) = \frac{(2\mu_C\mu_S + c_1)(2\sigma_{CS} + c_2)}{(\mu_C^2 + \mu_S^2 + c_1)(\sigma_C^2 + \sigma_S^2 + c_2)} \tag{14}$$

Here, c_1 and c_2 are two constants. In our case, these were set to 0.01 and 0.03 respectively. The average of $SSIM_i$, for $1 \le i \le (h \times w)/(d \times d)$, is regarded as a structural similarity index SSIM. Structural dissimilarity index is a distance matrix which is measured by Eq. (15) in each block.

$$SDIM_i = \frac{(1 - SSIM_i)}{2} \tag{15}$$

The average of these $SDIM_i$ is treated as structural dissimilarity index value, SDIM.

Fig. 11a,b depicts the quantity of implanted bits per one unit loss of structural similarity index value (i.e., SDIM value) in SPP and BPP based schemes respectively. The figure states that for the same amount of dissimilarities, i.e., level of distortions, all the *n*-predictor policies implant more quantity of bits and this amount of embedded bits increases along with the increment in the number of predictors in the *n*-predictor scheme. Fig. 11c,d demonstrates how the schemes preserved the value of SSIM in the Lena image at different embedding capacities. The figure states that the proposed multi-predictor policies maintain higher similarity index. This implies that the proposed scheme manages better image quality.

Finally, analyzing these PSNR and SSIM, it can be concluded that *n*-predictor policies embed more quantity of bits for the same amount of image distortions in the CalTech101 image dataset.

3.4. *Performance evaluation of the schemes in different standard image datasets*

The *n*-predictor and the reviewed schemes are experimented by using different categories of image datasets including the USC-SIPI texture images, the USC-SIPI standard images, the CalTech101 images, the Natural images and the CRISP's satellite images. All the experiments are conducted in MATLAB. The same data stream is embedded into each of the collected images by all the literature reviewed and proposed embedding methods. The results are presented in this subsection by averaging the payloads, PSNRs and SSIMs separately for each image dataset. This subsection also analyzes the minimum and the maximum embedding gains in each of the image datasets for each of the schemes. Finally, the performances of *n*-prediction policies among themselves are presented.

3.4.1. *Analysis on embedding payloads in diverse image dataset*

The average payloads of all the SPP and BPP based schemes, obtained in different image datasets, are tabulated in Tables 5 and 6 respectively. The CalTech101 and the Satellite images provide higher embedding payloads while the Texture images present smallest payloads in all the image dataset and in the experimented schemes. Most of the CalTech101 images highlight a single object. Variations among the neighbor pixels in such single object highlighting frames are small in magnitude. This virtue helps the predictors to predict more accurately

Please cite this article in press as: A.H.M. Kamal, Mohammad M. Islam, Enhancing embedding capacity and stego image quality by employing multi predictors, Journal of Information Security and Applications (2016), doi: 10.1016/j.jisa.2016.08.005

Table 5 – Average payloads in SPP based schemes.

Schemes	CalTech101	Standard	Natural	Texture	Satellite
Tai	15,409	10,362	9,064	2,891	12,231
Wien	16,011	10,615	9,324	3,256	12,247
Weijen	9,735	4,710	5,152	987	9,834
Xiao2	18,067	13,458	11,808	4,112	13,980
Xiao3	18,880	14,477	12,903	4,511	14,533
Xiao4	18,282	13,770	12,114	4,248	14,130
2-predictor	17,739	13,017	11,243	4,419	13,760
3-predictor	19,519	15,301	12,917	5,756	15,170
4-predictor	20,641	16,785	14,354	6,421	16,210
5-predictor	22,780	19,678	16,814	8,080	18,146

and to enhance the quantity of the embeddable errors. Again, the Satellite images contain cloud like large gray regions where the pixel values are very close to each other. Consequently, the frequencies of embeddable errors of –1 and 0 rise significantly in these two categories of images. On the other hand, in the Texture images, greater transitions of pixel values between the pixels of each two neighbor regions are observed; whereas the Natural and the Standard images contain random pixel variations. Hence, the payloads in the images of these two categories are in moderate level.

In the comparisons of the schemes, it is investigated that the multi-predictor based schemes like the Xiao et al.'s and the *n*-predictor which belong to the SPP technique present higher embedding payloads. As a whole, our proposed *n*-prediction policies exhibit their superior performance on presenting better payloads in Table 5. The average payloads tabulated in Table 6 underpin that among the BBP techniques, the *n*-predictor policy notably dominates the competing schemes.

The payload gains of the proposed *n*-predictor policies are always positive and this is a few multiple of some of the competing ones. As a sample, payload gains in 3-predictor policy regarding each of its competing schemes are presented in Tables 7 and 8 for each image dataset. Table 7 states that minimum and maximum gains are 17% and 418% over Tai, 15% and 202% over Wien, 10% and 627% over Weijen, 12% and 103% over Xiao2, 14% and 68% over Xiao3, 13% and 91% over Xiao4. Table 8 presents the gains for BPP techniques. This table also affirms that minimum and maximum gains are 11% and 165% on Kamal, 15% and 153% on Leung, 18% and 175% on Wien, 14% and 183% on Tsai, 27% and 2930% on Mid, 471% and9233% regarding Truncation.

These afore discussions validate that the proposed scheme outperforms regarding the large volume of data implantation capability.

Table 6 – Average payloads in BPP based schemes.

Schemes	CalTech101	Standard	Natural	Texture	Satellite
Kamal	18,190	13,759	13,173	7,350	15,796
Leung	18,944	14,477	13,106	7,805	16,302
Wien	18,293	13,902	13,595	7,351	15,708
Tsai	18,163	13,516	12,494	7,370	15,806
Mid	11,525	7,568	6,933	1,732	9,825
P2:KL	25,376	22,643	20,652	14,690	22,643
P3:KLW	27,142	24,776	23,212	16,348	24,617
P4:KLWT	30,771	29,591	27,609	20,869	28,884
P5:KLWTM	30,099	29,161	27,028	20,454	28,169
Truncation	1,051	1,669	782	424	1,463

Table 7 – Payload gain of 3-predictor scheme over the others SPP schemes.

Gain of 3-predictor over the ↓	CalTech101		Standard		Natural		Texture		Satellite	
	Min	Max	Min	Max	Min	Max	Min	Max	Min	Max
Tai	24	123	18	329	19	193	44	418	17	136
Wien	19	120	15	191	20	189	41	202	17	138
Weijen	17	463	15	627	19	529	73	460	10	392
Xiao2	17	55	12	81	18	88	32	103	18	57
Xiao3	19	42	17	63	14	57	23	68	17	37
Xiao4	14	66	18	72	13	75	30	91	17	49

Please cite this article in press as: A.H.M. Kamal, Mohammad M. Islam, Enhancing embedding capacity and stego image quality by employing multi predictors, Journal of Information Security and Applications (2016), doi: 10.1016/j.jisa.2016.08.005

Table 8 – Payload gain of 3-predictor scheme over the others BPP schemes.

Gain of 3-predictor over the ↓	CalTech101		Standard		Natural		Texture		Satellite	
	Min	Max	Min	Max	Min	Max	Min	Max	Min	Max
Kamal	22	136	11	158	20	165	78	160	12	145
Leung	15	127	19	153	17	149	59	152	19	138
Wien	30	146	18	169	27	175	84	174	19	159
Tsai	23	158	14	182	24	183	86	183	16	165
Mid	47	1018	34	2475	41	1536	185	2930	27	1141
Truncation	1197	6762	471	6705	790	7093	1018	9233	763	5666

3.4.2. *Analysis on PSNRs in diverse image dataset*

Average PSNRs are tabulated in Tables 9 and 10 separately for SPP and BPP techniques respectively. Both the tables demonstrate that PSNR is higher in our proposed *n*-predictor policies. The PSNR of 50 dBm or more is observed only in the proposed schemes. These PSNR values validate that the proposed scheme preserves the image quality better than the others. The proposed predictor generates more quantity of embeddable errors. The embeddable errors are shifted by one unit for conceiving a message bit '1' while these remained unchanged by hiding a bit '0'. On the contrary, the non-embeddable errors must shift their values by one unit to aid in reversible mechanism. Thus, the improvement in the number of embeddable errors increases the quantity of unaltered pixel in the stego image regarding its cover pixels. Consequently, the proposed scheme demonstrates better PSNR values.

3.4.3. *Analysis on SSIMs in diverse image dataset*

A higher value of structural similarity index indicates better similarities between two compared images. Tables 11 and 12 show the SSIM values respectively in SPP and BPP techniques. Table 11 states that the values of SSIM in all *n*-predictor policies are either higher or much closed to others. Table 12 outlines a definite improvement in SSIM by the proposed scheme.

3.4.4. *Analysis on the effect of increasing the number of predictors in the* n*-predictor scheme*

The time complexity of the scheme is related to the number of used predictors because each predictor predicts pixels separately. If the image size is *t*, the time complexity of the *n*-predictor scheme will be $O(nt)$ while it is $O(t)$ for a single predictor based scheme. The data are embedded into the prediction errors. This data embedding complexity is $O(t)$ for all. Thus total time complexity of the *n*-predictor scheme is $O(nt + t)$ while it is $O(2t)$ for the other schemes. The $O(nt + t)$ is not a polynomial representation and, thus, current computers complete the whole process within very few seconds. In most embedding applications, the issue of improving the payloads and the image quality by a scheme is more important than its execution times

Table 9 – Average PSNRs in SPP based schemes.

Schemes	CalTech101	Standard	Natural	Texture	Satellite
Tai	49.412	49.039	48.918	48.453	49.215
Wien	49.467	49.071	48.941	48.478	49.216
Weijen	49.442	49.109	49.090	48.457	49.320
Xiao2	49.698	49.362	49.206	48.563	49.385
Xiao3	49.714	49.381	49.234	48.566	49.393
Xiao4	49.660	49.322	49.167	48.546	49.361
2-predictor	49.854	49.556	49.365	48.677	49.524
3-predictor	49.979	49.705	49.476	48.767	49.621
4-predictor	50.002	49.735	49.509	48.772	49.634
5-predictor	50.145	49.921	49.651	48.869	49.754

Table 10 – Average PSNRs in BPP based schemes.

Schemes	CalTech101	Standard	Natural	Texture	Satellite
Kamal	49.466	49.131	49.074	48.619	49.318
Leung	49.532	49.192	49.068	48.650	49.366
Wien	49.475	49.143	49.110	48.619	49.309
Tsai	49.467	49.115	49.020	48.620	49.326
Mid	48.935	48.667	48.613	48.241	48.854
P2:KL	50.289	50.085	49.935	49.306	50.077
P3:KLW	50.289	50.085	49.935	49.306	50.077
P4:KLWT	50.675	50.572	50.362	49.700	50.495
P5:KLWTM	50.604	50.530	50.303	49.664	50.422
Truncation	0.380	0.363	0.387	0.397	0.369

Please cite this article in press as: A.H.M. Kamal, Mohammad M. Islam, Enhancing embedding capacity and stego image quality by employing multi predictors, Journal of Information Security and Applications (2016), doi: 10.1016/j.jisa.2016.08.005

Table 11 – Average SSIMs in SPP based schemes.

Schemes	CalTech101	Standard	Natural	Texture	Satellite
Tai	0.493	0.450	0.360	0.157	0.389
Wien	0.495	0.452	0.361	0.158	0.390
Weijen	0.489	0.445	0.357	0.155	0.386
Xiao2	0.493	0.450	0.360	0.156	0.388
Xiao3	0.494	0.451	0.360	0.157	0.389
Xiao4	0.494	0.451	0.360	0.157	0.389
2-predictor	0.492	0.448	0.358	0.156	0.387
3-predictor	0.493	0.449	0.359	0.156	0.388
4-predictor	0.493	0.449	0.359	0.156	0.388
5-predictor	0.494	0.451	0.360	0.157	0.389

if the required time is not too long. Fig. 12 states that values of payload, PSNR and SSIM, as shown in Fig. 12a–c respectively, increase with the increment of the number of applied predictors. The reason is explained above. Among the image datasets, this shows lower performance in the texture images because in these images the variation of values between neighbor pixels is high. Frequently, sudden transition between two neighbor pixels occurs. Consequently, the performance of the predictors is poor there. The poor performance of the predictors increases the quantity of non-embeddable errors. This is also described above that with the increment of the non-embeddable errors, the quantity of unchanged pixels decreases. Therefore, the PSNR and the SSIM values decrease in this dataset. After all, it is investigated in these figures that the embedding performance regarding the payloads and PSNR values increases if the number of applied predictor is increased.

Finally, the above discussions ensure that the proposed *n*-predictor policies provide both higher payloads and better stego image quality.

4. Future works

Nguyen et al. (2015) proposed an embedding scheme where data embedment is performed into the pixel differences. This method, at first, measures the differences between pair of pixels in a block. The selection of pixels in each pair is performed by a defined rule. The scheme then generates symbols which are consisted of 3 bits secret message chunk, i.e., 0, 1, . . ., 7. These symbols are arranged according to their appearing frequencies. An optimal embedding modification direction table is built to maintain the image distortion due to symbol implantation at minimum level for most appeared symbols to maximum level for lowest appeared ones. The implantation is performed associating two embeddable pixel differences and thus, this hides 3 bits into each two embeddable differences. If that embedment will be performed into the prediction errors rather than the pixel differences and the *n*-prediction scheme will be applied, the method in Nguyen et al. (2015) will improve the embedding payloads significantly as well as the image quality because this will embed 3 bits per two embeddable errors and the *n*-predictor scheme will generate more embeddable errors. Hence, this will then increase the embedding capacity by at least 50%. In our next work, we will take the idea into an experiment.

We are not satisfied by only improving the frequency of embeddable errors because the *n*-predictor scheme still produces plenty of non-embeddable errors. Therefore, the scheme cannot implant message bit into many pixels. In addition, the non-embeddable errors definitely contribute to the stego image distortions. We aim to implant a bit into every pixel equally. In our second future work, we will propose a very innovative idea in the field of reversible data hiding arena where each error will certainly conceive a message bit. If each error hides a bit, the embedding capacity of single layer reversible data embedment process will be 1 bit per pixel (bpp). Achieving 1 bpp embedding capacity, while scheme's endeavor is to embed one bit per pixel, will be a unique contribution in this research arena.

5. Conclusions

The reversible schemes suffer from the lower embedding capacity. Nevertheless, many applications related to forensic,

Table 12 – Average SSIMs in BPP based schemes.

Schemes	CalTech101	Standard	Natural	Texture	Satellite
Kamal	0.520	0.459	0.372	0.157	0.400
Leung	0.521	0.461	0.373	0.159	0.403
Wien	0.527	0.467	0.380	0.162	0.408
Tsai	0.524	0.464	0.375	0.161	0.405
Mid	0.527	0.467	0.378	0.162	0.405
P2:KL	0.528	0.469	0.380	0.163	0.408
P3:KLW	0.529	0.470	0.381	0.163	0.409
P4:KLWT	0.532	0.474	0.384	0.165	0.411
P5:KLWTM	0.533	0.475	0.385	0.166	0.412
Truncation	0.034	0.024	0.040	0.137	0.202

Please cite this article in press as: A.H.M. Kamal, Mohammad M. Islam, Enhancing embedding capacity and stego image quality by employing multi predictors, Journal of Information Security and Applications (2016), doi: 10.1016/j.jisa.2016.08.005

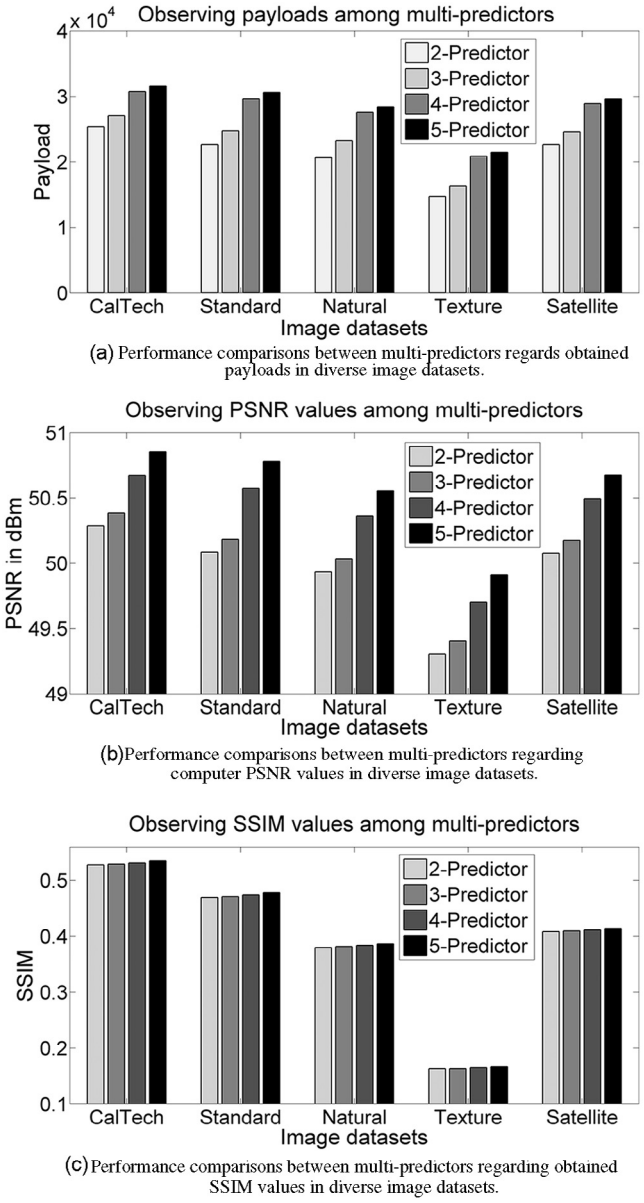

(a) Performance comparisons between multi-predictors regards obtained payloads in diverse image datasets.

(b) Performance comparisons between multi-predictors regarding computer PSNR values in diverse image datasets.

(c) Performance comparisons between multi-predictors regarding obtained SSIM values in diverse image datasets.

Fig. 12 – Observing the effects of uses of more multi-predictors on performance measuring parameters.

medical, and military and law enforcing agencies utilize both the extracted secrets and the retrieved cover image to their further processing stages at their decoder end. Consequently, in this arena, increasing the embedding capacity and the stego image quality is an attractive area for the researcher. The proposed *n*-predictor scheme increases the embedding capacity notably. The scheme is experimented on five different image datasets. These reveal that it enhances the embedding capacity of SPP techniques by 10%–627% and BPP techniques by 11%–9233% depending on the texture properties and pixel variations in the images. The self-reliant decoder can extract these secrets and retrieve the cover image from the stego one. Therefore, it will be an effective method to meet the demand for larger embedding capacity. The analyses on both the PSNR and SSIM, in this article, ensure that this scheme minimizes the distortions in the stego image compared to its competing schemes. Besides, the use of multiple predictors will increase the security of the scheme as the list of the applied predictors, predictors' own parameters and their application sequences are not open to any third party.

Conflict of interest

The authors do not have any economical interest from that article. The first author is a PhD student and working under the supervision of the second author. To meet the requirement for achieving the PhD degree, the first author has to publish his research works on ranked journals which are published by well recognized publishers. Therefore, the authors have chosen this journal to publish that work. Both the authors are aware of that submission. The first author is a fellow of ICT Division of the Ministry of Post, Telecommunication and Information Technology of the Government of Bangladesh. However, the fellowship neither covers any publication charges nor claims any financial interest from that research.

Author's contributions

The first author, AHMK, is a PhD student of the Department of Computer Science and Engineering of the Bangladesh University of Engineering and Technology. He is working under the supervision of the second author, MMI. Hence, the whole work is supervised and guided by MMI. Mr. MMI has been consulted on all the way to the progress of the research work by the author AHMK. Mr. AHMK has completed the experiments and drafted the manuscript. Mr. MMI has revised the manuscript and given the final approval to submit it to this journal.

Acknowledgments

The author AHMK is funded by the ICT Division of the Ministry of Post, Telecommunication and Information Technology of the Government of Bangladesh through a fellowship program. Therefore, the authors would like to acknowledge the State Ministry of Bangladesh.

REFERENCES

Böhme R, Kirchner M. Counter-forensics: attacking image forensics. Digit Image Forensics 2013;327–66.

Brindha S, Vennila I. Hiding fingerprint in face using scattered LSB embedding steganographic technique for smart card based authentication system. Int J Comput Appl 2011;26(10):51–5.

Chao RM, Wu HC, Lee CC, Chu YP. A novel image data hiding scheme with diamond encoding. EURASIP J Inform Sec 2009;2009:658047.

Chen X, Sun X, Sun H, Zhou Z, Zhang J. Reversible watermarking method based on asymmetric-histogram shifting of prediction errors. J Syst Softw 2013;86(10):2620–6.

Chien-Chang C, Tsai Y-H. Adaptive reversible image watermarking scheme. J Syst Softw 2011;84(3):428–34.
Chung K-L, Huang Y-H, Yan W-M, Teng W-C. Distortion reduction for histogram modification-based reversible data hiding. Appl Math Comput 2012;218(9):5819–26.
Fei-Fei L, Fergus R, Perona P. Learning generative visual models from few training examples: an incremental Bayesian approach tested on 101 object categories. In: IEEE. CVPR 2004, Workshop on Generative-Model Based Vision; 2004.
Fridrich J, Goljan M, Du R. Lossless data embedding for all image formats. In: Electronic Imaging 2002. International Society for Optics and Photonics; 2002.
Gujjunoori S, Amberker BB. DCT based reversible data embedding for MPEG-4 video using HVS characteristics. J Inform Sec Appl 2013;18(4):157–66.
Hong W. Adaptive reversible data hiding method based on error energy control and histogram shifting. Opt Commun 2012;285(2):101–8.
Hong W, Chen T-S. A local variance-controlled reversible data hiding method using prediction and histogram-shifting. J Syst Softw 2010;83(12):2653–63.
Hong W, Chen T-S. A novel data embedding method using adaptive pixel pair matching. IEEE Trans Inf Forensics Security 2012;7(1):176–84.
Hong W, Chen T-S, Luo C-W. Data embedding using pixel value differencing and diamond encoding with multiple-base notational system. J Syst Softw 2012;85(5):1166–75.
I-Cheng C, Hu Y-C, Chen W-L, Lo C-C. High capacity reversible data hiding scheme based on residual histogram shifting for block truncation coding. Signal Process 2015;108:376–88.
Kamal AHM. Steganography: securing message in wireless network. Int J Comput Technol 2013;4(3):797–801.
Kamal AHM, Islam MM. Capacity improvement of reversible data hiding scheme through better prediction and double cycle embedding process. In: Proc. IEEE Int Conference on Advance Networks and Telecommunication Systems; 2015 (accepted).
Kamal AHM, Islam MM. Enhancing the embedding payload by handling the affair of association and mapping of block pixels through prediction errors histogram. In: Proc. of Int Conference on Networks Systems and Security; 2016a.
Kamal AHM, Islam MM. Boosting up the data hiding rate multi cycle embedment process. J Vis Commun Image R 2016b;doi:10.1016/j.jvcir.2016.07.023.
Kamal AHM, Mahfuzul Islam M. Facilitating and securing offline e-medicine service through image steganography. Healthc Technol Lett 2014;1(2):74–9.
Kamstra L, Heijmans HJAM. Reversible data embedding into images using wavelet techniques and sorting. IEEE Trans Image Process 2005;14(12):2082–90.
Lee C-F, Chen H-L. A novel data hiding scheme based on modulus function. J Syst Softw 2010;83(5):832–43.
Lee J-D, Chiou Y-H, Guo J-M. Information hiding based on block match coding for vector quantization-compressed images. IEEE Syst J 2014;8(3):737–48.
Leung HY, Cheng LM, Liu F, Fu QK. Adaptive reversible data hiding based on block median preservation and modification of prediction errors. J Syst Soft 2013;86(8):2204–19.
Lin C-C. An information hiding scheme with minimal image distortion. Comp Stand Inter 2011;33(5):477–84.
Liu C-L, Liao S-R. High-performance JPEG steganography using complementary embedding strategy. Pattern Recognit 2008;4(19):2945–55.
Lu Y-Y, Huang H-C. Adaptive reversible data hiding with pyramidal structure. Vietnam J Comput Sci 2014;1–13.
Lu Z-M, Wang J-X, Liu B-B. An improved lossless data hiding scheme based on image VQ-index residual value coding. J Syst Softw 2009;82(6):1016–24.
Luo W, Wang Y, Huang J. Security analysis on spatial 1 steganography for JPEG decompressed images. IEEE Signal Process Lett 2011;18(1):39–42.
Ma X, Pan Z, Hu S, Wang L. High-fidelity reversible data hiding scheme based on multi-predictor sorting and selecting mechanism. J Vis Commun Image R 2015;28:71–82.
Nguyen T-S, Chang C-C, Huynh N-T. A novel reversible data hiding scheme based on difference-histogram modification and optimal EMD algorithm. J Vis Commun Image R 2015;33:389–97.
Ong SY, Wong K, Tanaka K. A scalable reversible data embedding method with progressive quality degradation functionality. Signal Process Image Commun 2014;29(1):135–49.
Ou B, Li X, Zhao Y, Ni R. Reversible data hiding based on PDE predictor. J Syst Softw 2013;86(10):2700–9.
Provos N, Honeyman P. Hide and seek: an introduction to steganography. IEEE Secur Priv 2003;1(3):32–44.
Tai W-L, Yeh C-M, Chang C-C. Reversible data hiding based on histogram modification of pixel differences. IEEE Trans Circuits Syst Video Technol 2009;19(6):906–10.
Tsai P, Hu Y-C, Yeh H-L. Reversible image hiding scheme using predictive coding and histogram shifting. Signal Process 2009;89(6):1129–43.
Ulutas M, Ulutas G, Nabiyev VV. Medical image security and EPR hiding using Shamir's secret sharing scheme. J Syst Soft 2011;84(3):341–53.
Wang W-J, Huang C-T, Wang S-J. VQ applications in steganographic data hiding upon multimedia images. IEEE Syst J 2011;5(4):528–37.
Wang XT, Chang CC, Nguyen TS, Li MC. Reversible data hiding for high quality image exploiting interpolation and direction order mechanism. Digit Sig Proc 2013;23(2):569–77.
Wang Z, Lee C-F, Chang C-Y. Histogram-shifting-imitated reversible data hiding. J Syst Softw 2013;86(2):315–23.
Weng C-Y, Zhang YH, Lin LC, Wang S-J. Visible watermarking images in high quality of data hiding. Sci and Bus Media 2013;66:1033.
Yang CH, Weng CY, Wang SJ, Sun HM. Varied PVD+ LSB evading detection programs to spatial domain in data embedding systems. J Syst Softw 2010;83(10):1635–43.
Yang WJ, Chung KL, Liao HY, Yu WK. Efficient reversible data hiding algorithm based on gradient-based edge direction prediction. J Syst Softw 2013;86(2):567–80.
Zhou Wang ACB. A universal image quality index. IEEE Signal Process Lett 2002;9:81–4.

A.H.M. Kamal is with the Department of Computer Science and Engineering (CSE), Bangladesh University of Engineering and Technology (BUET), Dhaka, Bangladesh, as a PhD student and on study leave from the Department of CSE, Jatiya Kabi Kazi Nazrul Islam University, Trishal, Mymensingh, P.C. 2220, Bangladesh (e-mail: ahmkctg@yahoo.com, kamal@jkkniu.edu.bd).

Mohammad M. Islam is a professor of the Department of CSE, BUET (e-mail: mahfuz@cse.buet.ac.bd).

Please cite this article in press as: A.H.M. Kamal, Mohammad M. Islam, Enhancing embedding capacity and stego image quality by employing multi predictors, Journal of Information Security and Applications (2016), doi: 10.1016/j.jisa.2016.08.005